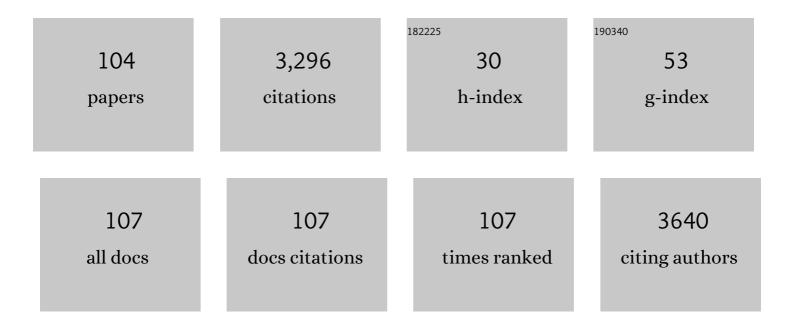
List of Publications by Year in descending order

Source: https://exaly.com/author-pdf/176895/publications.pdf Version: 2024-02-01



#	Article	IF	CITATIONS
1	High-quality graphene from the surface of CrFeCoNiC high-entropy alloy. Journal of Alloys and Compounds, 2022, 889, 161712.	2.8	1
2	NiFe Layered Double Hydroxides Grown on a Corrosionâ€Cell Cathode for Oxygen Evolution Electrocatalysis. Advanced Energy Materials, 2022, 12, 2102372.	10.2	51
3	NiFe Layered Double Hydroxides Grown on a Corrosionâ€Cell Cathode for Oxygen Evolution Electrocatalysis (Adv. Energy Mater. 2/2022). Advanced Energy Materials, 2022, 12, .	10.2	6
4	High-entropy induced a glass-to-glass transition in a metallic glass. Nature Communications, 2022, 13, 2183.	5.8	34
5	Intrinsic fast kinetics on the degradation of azo dye by iron in alkaline condition. Chemical Engineering Journal Advances, 2022, , 100321.	2.4	0
6	Theoretical and experimental study of metallic glass die-imprinting for manufacturing large-size micro/nano structures. Journal of Materials Processing Technology, 2022, 307, 117699.	3.1	4
7	Pressure-induced local structural crossover in a high-entropy metallic glass. Physical Review B, 2022, 105, .	1.1	2
8	Segregating the homogeneous passive film and understanding the passivation mechanism of Ti-based metallic glasses. Corrosion Science, 2021, 178, 109078.	3.0	19
9	Magical oxygen: Tuning Cu&Ag nanoporous membrane into nanoporous (Cu&Ag)@Ag core-shell alloy. Physica B: Condensed Matter, 2021, 614, 413011.	1.3	4
10	Cheap, fast and durable degradation of azo dye wastewater by zero-valent iron structural composites. Journal of Environmental Chemical Engineering, 2021, 9, 106314.	3.3	7
11	Stress-induced activation of the commercial Fe-based metallic glass ribbons for azo dye degradation. Journal of Non-Crystalline Solids, 2021, 572, 121117.	1.5	3
12	Effect of TiC Addition on the High-Temperature Hardness and the Carbide Stability in Al0.2CoCrFeNi1.5Ti High-Entropy Alloy. Russian Journal of Non-Ferrous Metals, 2021, 62, 708-715.	0.2	0
13	Excellent long-term reactivity of inhomogeneous nanoscale Fe-based metallic glass in wastewater purification. Science China Materials, 2020, 63, 453-466.	3.5	22
14	An abnormal correlation between electron work function and corrosion resistance in Ti-Zr-Be-(Ni/Fe) metallic glasses. Corrosion Science, 2020, 165, 108392.	3.0	29
15	Effect of Mo Addition on The Microstructure and Mechanical Properties of CoCuFeNi High Entropy Alloy. Metals, 2020, 10, 1017.	1.0	8
16	Nanoporous silver using pulsed laser deposition for high-performance oxygen reduction reaction and hydrogen peroxide sensing. Nanoscale, 2020, 12, 19413-19419.	2.8	14
17	How does the structural inhomogeneity influence the shear band behaviours of metallic glasses. Philosophical Magazine, 2020, 100, 1663-1681.	0.7	3
18	Phase stabilities of high entropy alloys. Scripta Materialia, 2020, 179, 40-44.	2.6	51

#	Article	IF	CITATIONS
19	Porous composite architecture bestows Fe-based glassy alloy with high and ultra-durable degradation activity in decomposing azo dye. Journal of Hazardous Materials, 2020, 388, 122043.	6.5	20
20	Unique energy-storage behavior related to structural heterogeneity in high-entropy metallic glass. Materials Science & Engineering A: Structural Materials: Properties, Microstructure and Processing, 2020, 786, 139417.	2.6	15
21	Cryogenic charpy impact toughness of (Ti41Zr25Be26Ni8)93Cu7 bulk metallic glass. Materials Science & Engineering A: Structural Materials: Properties, Microstructure and Processing, 2020, 786, 139442.	2.6	10
22	The novel Ti-based metallic glass with excellent glass forming ability and an elastic constant dependent glass forming criterion. Materialia, 2019, 8, 100433.	1.3	14
23	Novel corrosion behaviours of the annealing and cryogenic thermal cycling treated Ti-based metallic glasses. Intermetallics, 2019, 110, 106467.	1.8	23
24	Scalable preparation of hierarchical porous activated carbon/graphene composites for high-performance supercapacitors. Journal of Materials Chemistry A, 2019, 7, 10058-10066.	5.2	19
25	Centimeter-sized Ti-rich bulk metallic glasses with superior specific strength and corrosion resistance. Journal of Non-Crystalline Solids, 2019, 512, 206-210.	1.5	18
26	Understanding the Fracture Behaviors of Metallic Glasses—An Overview. Applied Sciences (Switzerland), 2019, 9, 4277.	1.3	11
27	In-situ synthesis, operation and regeneration of nanoporous silver with high performance toward oxygen reduction reaction. Nano Energy, 2019, 58, 69-77.	8.2	27
28	Electrochemical corrosion resistance of the amorphous and crystalline Pdâ€based alloys in simulated seawater. Materials and Corrosion - Werkstoffe Und Korrosion, 2018, 69, 1509-1515.	0.8	2
29	The effect of void defects on the shear band nucleation of metallic glasses. Intermetallics, 2018, 94, 114-118.	1.8	21
30	Hierarchically Mesostructured Aluminum Current Collector for Enhancing the Performance of Supercapacitors. ACS Applied Materials & amp; Interfaces, 2018, 10, 16572-16580.	4.0	32
31	Microstructures and Mechanical Properties of AlCrFeNiMo <sub>0.5</sub> Ti <sub> <i>x</i> </sub> High Entropy Alloys. Chinese Physics Letters, 2018, 35, 036102.	1.3	5
32	Microstructures and mechanical properties of Ti NbMoTaW refractory high-entropy alloys. Materials Science & Engineering A: Structural Materials: Properties, Microstructure and Processing, 2018, 712, 380-385.	2.6	209
33	Structures and corrosion properties of the AlCrFeNiMo <sub>0.5</sub> Ti <sub><i>x</i></sub> high entropy alloys. Materials and Corrosion - Werkstoffe Und Korrosion, 2018, 69, 641-647.	0.8	28
34	High-Performance Carbon Dioxide Electrocatalytic Reduction by Easily Fabricated Large-Scale Silver Nanowire Arrays. ACS Applied Materials & Interfaces, 2018, 10, 17950-17956.	4.0	51
35	Fe-based multi-phase nanocrystalline ribbons with hierarchically flowerlike structured metal oxides after modified by Orange II for CrVI absorption. Journal of Iron and Steel Research International, 2018, 25, 608-613.	1.4	4
36	Fabrication and molecular dynamics analyses of highly thermal conductive reduced graphene oxide films at ultra-high temperatures. Nanoscale, 2017, 9, 2340-2347.	2.8	71

#	Article	IF	CITATIONS
37	Experimental and Correlative Analyses of the Ageing Mechanism of Activated Carbon Based Supercapacitor. Electrochimica Acta, 2017, 228, 214-225.	2.6	46
38	Effect of Ti additions on mechanical properties of NbMoTaW and VNbMoTaW refractory high entropy alloys. Intermetallics, 2017, 84, 153-157.	1.8	289
39	Understanding the effects of Poisson's ratio on the shear band behavior and plasticity of metallic glasses. Journal of Materials Science, 2017, 52, 6789-6799.	1.7	14
40	Unexpected high performance of Fe-based nanocrystallized ribbons for azo dye decomposition. Journal of Materials Chemistry A, 2017, 5, 14230-14240.	5.2	74
41	Oxide-derived nanostructured metallic-glass electrodes for efficient electrochemical hydrogen generation. RSC Advances, 2017, 7, 27058-27064.	1.7	17
42	The multiple shear bands and plasticity in metallic glasses: A possible origin from stress redistribution. Journal of Alloys and Compounds, 2017, 695, 3457-3466.	2.8	17
43	One-pot preparation of nanoporous Ag-Cu@Ag core-shell alloy with enhanced oxidative stability and robust antibacterial activity. Scientific Reports, 2017, 7, 10249.	1.6	29
44	Effects of Cu addition on the glass forming ability and corrosion resistance of Ti-Zr-Be-Ni alloys. Journal of Alloys and Compounds, 2017, 725, 573-579.	2.8	37
45	Effect of residual stress on azo dye degradation capability of Fe-based metallic glass. Journal of Non-Crystalline Solids, 2017, 473, 74-78.	1.5	29
46	Size effect in Pd77.5Cu6Si16.5 metallic glass micro-wires: More scattered strength with decreasing diameter. Applied Physics Letters, 2017, 111, .	1.5	7
47	Multi-phase nanocrystallization induced fast degradation of methyl orange by annealing Fe-based amorphous ribbons. Intermetallics, 2017, 90, 30-35.	1.8	34
48	Serration Behavior of a Zr-Based Metallic Glass Under Different Constrained Loading Conditions. Metallurgical and Materials Transactions A: Physical Metallurgy and Materials Science, 2016, 47, 5395-5400.	1.1	13
49	The shear band controlled deformation in metallic glass: a perspective from fracture. Scientific Reports, 2016, 6, 21852.	1.6	22
50	Serration behaviours in metallic glasses with different plasticity. Philosophical Magazine, 2016, 96, 2243-2255.	0.7	23
51	The material-dependence of plasticity in metallic glasses: An origin from shear band thermology. Materials and Design, 2016, 96, 189-194.	3.3	13
52	A non-viscous-featured fractograph in metallic glasses. Philosophical Magazine, 2016, 96, 542-550.	0.7	2
53	A study of cooling process in bulk metallic glasses fabrication. AIP Advances, 2015, 5, .	0.6	14
54	Microstructure, phase stability and mechanical properties of Nb–Ni–Ti–Co–Zr and Nb–Ni–Ti–Co–Zr–Hf high entropy alloys. Progress in Natural Science: Materials International, 2015, 25, 365-369.	1.8	33

#	Article	IF	CITATIONS
55	Morphology and structure evolution of metallic nanowire arrays prepared by die nanoimprinting. Science Bulletin, 2015, 60, 629-633.	4.3	9
56	Effects of austenitizing temperature on the microstructure and electrochemical behavior of a martensitic stainless steel. Journal of Applied Electrochemistry, 2015, 45, 375-383.	1.5	31
57	Fe-based bulk amorphous alloys with high glass formation ability and high saturation magnetization. Science Bulletin, 2015, 60, 396-399.	4.3	21
58	Insight into the high reactivity of commercial Fe–Si–B amorphous zero-valent iron in degrading azo dye solutions. RSC Advances, 2015, 5, 34032-34039.	1.7	96
59	Highâ€accuracy bulk metallic glass mold insert for hot embossing of complex polymer optical devices. Journal of Polymer Science, Part B: Polymer Physics, 2015, 53, 463-467.	2.4	16
60	Rapid decomposition of Direct Blue 6 in neutral solution by Fe–B amorphous alloys. RSC Advances, 2015, 5, 6215-6221.	1.7	96
61	Pseudo-quinary Ti20Zr20Hf20Be20(Cu20-xNix) high entropy bulk metallic glasses with large glass forming ability. Materials and Design, 2015, 87, 625-631.	3.3	83
62	Fabrication of CrSi2/MoSi2/SiC–Mo2C gradient composite coating on Mo substrate and the stabilizing effect of Cr on the coating's anti-oxidation properties. Surface and Coatings Technology, 2015, 282, 188-199.	2.2	15
63	Experimental and Theoretical Advances in Amorphous Alloys. Advances in Materials Science and Engineering, 2014, 2014, 1-2.	1.0	6
64	Atomic structure and bonding of the interfacial bilayer between Au nanoparticles and epitaxially regrown MgAl2O4 substrates. Applied Physics Letters, 2014, 105, .	1.5	16
65	Nanocrystalline Phase Formation inside Shear Bands of Pd-Cu-Si Metallic Glass. Advances in Materials Science and Engineering, 2014, 2014, 1-4.	1.0	4
66	Direct experimental evidence of nano-voids formation and coalescence within shear bands. Applied Physics Letters, 2014, 105, 181909.	1.5	51
67	Novel Ti <sub>3</sub> Sn based high damping material with high strength. Materials Research Innovations, 2014, 18, S4-584-S4-587.	1.0	2
68	A Centimeter-Sized Quaternary Ti-Zr-Be-Ag Bulk Metallic Glass. Advances in Materials Science and Engineering, 2014, 2014, 1-5.	1.0	6
69	In-situ fabrication of MoSi2/SiC–Mo2C gradient anti-oxidation coating on Mo substrate and the crucial effect of Mo2C barrier layer at high temperature. Applied Surface Science, 2014, 308, 261-268.	3.1	32
70	A senary TiZrHfCuNiBe high entropy bulk metallic glass with large glass-forming ability. Materials Letters, 2014, 125, 151-153.	1.3	112
71	Facile synthesis of air-stable nano/submicro dendritic copper structures and their anti-oxidation properties. RSC Advances, 2014, 4, 33362-33365.	1.7	12
72	Large-area and uniform amorphous metallic nanowire arrays prepared by die nanoimprinting. Journal of Alloys and Compounds, 2014, 605, 7-11.	2.8	26

#	Article	IF	CITATIONS
73	Fabrication and microwave absorption properties of carbon-coated cementite nanocapsules. Nanotechnology, 2014, 25, 035704.	1.3	36
74	Highly Uniform and Reproducible Surface Enhanced Raman Scattering on Air-stable Metallic Glassy Nanowire Array. Scientific Reports, 2014, 4, 5835.	1.6	86
75	A New Centimeterâ€Sized Tiâ€Based Quaternary Bulk Metallic Glass with Good Mechanical Properties. Advanced Engineering Materials, 2013, 15, 691-696.	1.6	21
76	Ti-Zr-Be-Fe quaternary bulk metallic glasses designed by Fe alloying. Science China: Physics, Mechanics and Astronomy, 2013, 56, 2090-2097.	2.0	12
77	A Ti–Zr–Be–Fe–Cu bulk metallic glass with superior glass-forming ability and high specific strength. Intermetallics, 2013, 43, 177-181.	1.8	45
78	The effect of simulated thermal cycling on thermal and mechanical stability of a Ti-based bulk metallic glass. Journal of Alloys and Compounds, 2013, 575, 449-454.	2.8	32
79	Preparation of Fe–Ni–P–B metallic nano-ribbons. Materials Letters, 2013, 93, 103-106.	1.3	7
80	Ultrafine eutectic Ti x Sn y /TiNi composites with high damping capacity. Rare Metals, 2013, 32, 196-200.	3.6	3
81	Structural investigation of interface and defects in epitaxial Bi3.25La0.75Ti3O12 film on SrRuO3/SrTiO3 (111) and (100). Journal of Applied Physics, 2013, 113, 044102.	1.1	2
82	Two-zone heterogeneous structure within shear bands of a bulk metallic glass. Applied Physics Letters, 2013, 103, .	1.5	43
83	Effects of Fe addition on glass-forming ability and mechanical properties of Ti–Zr–Be bulk metallic glass. Journal of Alloys and Compounds, 2012, 536, 26-29.	2.8	70
84	Centimeter-sized Ti-based bulk metallic glass with high specific strength. Progress in Natural Science: Materials International, 2012, 22, 401-406.	1.8	24
85	Lightweight Ti–Zr–Be–Al bulk metallic glasses with improved glass-forming ability and compressive plasticity. Journal of Non-Crystalline Solids, 2012, 358, 2620-2625.	1.5	30
86	Effect of thermal cycling on the mechanical properties of Zr41Ti14Cu12.5Ni10Be22.5 alloy. Science China: Physics, Mechanics and Astronomy, 2012, 55, 2357-2361.	2.0	22
87	Chemical composition dependence of atomic oxygen erosion resistance in Cu-rich bulk metallic glasses. Science Bulletin, 2012, 57, 4801-4804.	1.7	6
88	Effect of alternating voltage treatment on corrosion resistance of AZ91D magnesium alloy. Materials and Corrosion - Werkstoffe Und Korrosion, 2012, 63, 505-516.	0.8	10
89	Effect of hydrostatic pressure on the nature of passive film of pure nickel. Materials and Corrosion - Werkstoffe Und Korrosion, 2011, 62, 269-274.	0.8	7
90	Atomic structure of T1 precipitates in Al–Li–Cu alloys revisited with HAADF-STEM imaging and small-angle X-ray scattering. Acta Materialia, 2011, 59, 462-472.	3.8	198

#	Article	IF	CITATIONS
91	Effects of the Cooling Rate on the Plasticity of Pd <sub>40.5</sub> Ni <sub>40.5</sub> P <sub>19</sub> Bulk Metallic Glasses. Chinese Physics Letters, 2011, 28, 116104.	1.3	10
92	Imaging, Core-Loss, and Low-Loss Electron-Energy-Loss Spectroscopy Mapping in Aberration-Corrected STEM. Microscopy and Microanalysis, 2010, 16, 416-424.	0.2	36
93	Quantification of the Ti oxidation state in BaTi1â^xNbxO3 compounds. Ultramicroscopy, 2010, 110, 1014-1019.	0.8	32
94	A stochastic analysis of the effect of magnetic field on the pitting corrosion susceptibility of pure magnesium. Materials and Corrosion - Werkstoffe Und Korrosion, 2010, 61, 306-312.	0.8	6
95	Corrosion behavior of Mgâ€10Gdâ€2Yâ€0.4Zr alloy under thin electrolyte layers. Materials and Corrosion - Werkstoffe Und Korrosion, 2010, 61, 388-397.	0.8	5
96	Coexistence of A―and Bâ€5ite Vacancy Compensation in Laâ€Doped Sr <sub>1â^'<i>x</i></sub> Ba <i><sub>x</sub></i> TiO <sub>3</sub> . Journal of the American Ceramic Society, 2010, 93, 2903-2908.	1.9	16
97	The role of lattice misfit strains in the deposition of epitaxial (Ba1â^'ySry)Ti0.5Nb0.5O3 films. Journal of Crystal Growth, 2009, 311, 2753-2758.	0.7	1
98	Applications of Aberration-corrected TEM and STEM in Complex Oxides and Nanostructured Materials. Microscopy and Microanalysis, 2009, 15, 154-155.	0.2	13
99	Structural and transport properties of epitaxial niobium-doped BaTiO3 films. Applied Physics Letters, 2008, 93, 192114.	1.5	21
100	Sr ion distribution and local structure in La1â^'xSrxMnO3. Journal of Physics Condensed Matter, 2006, 18, 5579-5586.	0.7	8
101	Organic Solid Solutions: Formation and Applications in Organic Light-Emitting Diodes. Advanced Functional Materials, 2005, 15, 1781-1786.	7.8	30
102	Efficient Organic Heterojunction Photovoltaic Cells Based on Triplet Materials. Advanced Materials, 2005, 17, 2841-2844.	11.1	267
103	Simulation of Structural Parameters and Superconducting Transition Temperature of MgB <sub>2</sub> under Pressure. Materials Science Forum, 2005, 475-479, 3319-3322.	0.3	0
104	The pressure dependence of the structure and superconducting transition temperature of MgB2. Journal of Physics Condensed Matter, 2004, 16, 1103-1113.	0.7	12